JOURNAL OF MATERIALS SCIENCE 18 (1983) 3661–3670

The martensitic transformation in cold-worked Fe–Mn alloys studied by Mössbauer spectroscopy

F. GAUZZI, B. VERDINI
Istituto di Metallurgia, Università di Roma, Via Eudossiana 18, Roma, Italy
G. PRINCIPI, B. BADAN
Istituto di Chimica Industriale, Università di Padova, Via Marzolo 9, Padova, Italy

The effect of cold-working on 16, 23 and 30 at % Mn iron–manganese alloys (C < 0.05 at %) has been examined using Mössbauer spectroscopy and X-ray diffractometry. The induced martensitic transformation $\gamma \rightarrow \epsilon, \alpha'$ depends on the composition and on the initial structure. It is found that the $\gamma \rightarrow \alpha'$ transformation in presence of the ϵ phase occurs only at high deformations.

1. Introduction

The existence in the Fe–Mn–C system (Mn > 10 at %) of the martensitic ϵ (h c p) and α' (b c c) phases alongside γ austenite (f c c) has been well known for some time. Each of these phases can transform into one of the others in alloys of given compositions on subjection to suitable thermal or thermomechanical treatment. In particular the simple cold-working of alloys with a manganese content ~ 15 to 30 at % induces the partial or total substitution of γ austenite by the ϵ and α' phases, whose relative amounts depend both on the alloy composition and on the deformation undergone.

The aim of this work is to apply the Mössbauer technique to the evolution of the phase distribution due to the plastic deformation of this kind of alloy and in particular to study the mechanism of the $\gamma \rightarrow \alpha'$ transformation in the presence or absence of ϵ. With this aim we prepared alloys with a nominal mean composition ~ 16, 23 and 30 at % Mn in order to obtain the starting structures $\gamma + \epsilon + \alpha'$, $\gamma + \epsilon$ and γ alone, respectively.

The Mössbauer characterization of the Fe–Mn–C system has been the object of several works. In particular Ishikawa and Endo [1] have found that the γ austenite is antiferromagnetic, having a Néel temperature above room temperature (~ 430 K for the 30 at % Mn alloy): the spectrum profile is therefore a magnetic sextet which, however, is not well resolved even at 20 K. The internal field at 0 K has the value $H_{int} = 41 \pm 3$ kG and its variation with the temperature is independent of the manganese concentration. Belozerskiy and co-workers [2] have suggested that iron atoms in the f c c lattice may be present both in the antiferromagnetic and in the paramagnetic states depending on the cooling rate after annealing at 1100° C: a very slow cooling would promote the formation of paramagnetic γ. Nevertheless a direct comparison with other experimental data is difficult owing to the lack of quantitative indications on the cooling rates used.

According to Ohno and Mekata [3], the ϵ phase, which is paramagnetic at room temperature, is a doublet with a quadrupole splitting of 0.14 mm sec^{-1} and an isomer shift referred to α-iron of − 0.20 mm sec^{-1} (values extrapolated to 0 at % Mn).

The ferromagnetic α' phase is characterized by a more complex Mössbauer pattern: the ferromagnetic sextet displays a broadening of the outer lines when the manganese content exceeds 8 at %. The spectrum for single phase alloys (α' only) has been interpreted by Litvinov and co-workers [4] as being made up of several ferromagnetic components due to the additive contribution of manganese atoms in the first three coordination

0022–2461/83 $03.00 + .12

spheres of the iron atoms. In the determination of the H_{int} of the α' phase in the presence of other phases (γ and ϵ) only the nearest neighbours were taken into account by those authors. On the other hand, Barton *et al.* [5] considered the α' spectrum as being composed of three subspectra attributed to iron atoms with 0, 1 and 2 or 3 manganese atoms as nearest neighbours. Here we have adopted this last model as being suitable for bringing out the influence of the manganese concentration on the features of the α' spectrum.

2. Experimental details

We studied the Fe–Mn–C alloys, whose compositions are given in Table I. The alloys were obtained by melting Armco iron (C < 0.05 at%) and electrolytic manganese (99 at%) in vacuo (pressure $\leqslant$ 1.3 mPa) and using a suitable technique to control the manganese loss by evaporation [6]. After solidification, ingots of about 150 g were repeatedly forged at about 1000° C to obtain homogenized plates 3 to 5 mm thick. The thickness was then reduced to about 500 μm by repeated cold-working alternated with vacuum annealing at ~ 1000° C. As a consequence of such treatment some inhomogeneity in the final samples is foreseeable. Table I gives the analytical compositions at this step of the preparation. The samples were then cold-worked and the mean value of deformation was determined by measuring the thickness variation at several points.

The samples to be analysed in Mössbauer transmission geometry (A-type) were chemically thinned with 10% H_3PO_4 in H_2O_2 ($T = 60°$ C) to a thickness of about 30 to 40 μm. Some samples were thinned only on one side (B-type), the other side being shielded by Lacomit varnish. The unthinned samples (C-type) were analysed in backscattering geometry. The samples were tested by X-ray diffractometry (Mo$K\alpha$ and Fe$K\alpha$) as a check on their structure.

The Mössbauer analysis was carried out at room temperature by means of a conventional spectrometer with constant acceleration movement, using a ^{57}Co/Rh source of 100 mCi nominal activity.

TABLE I Chemical compositions of the alloys examined (at%)

Alloy	Mn	C
X1Mn16	16.1	< 0.05
X1Mn23	23.4	< 0.05
X1Mn30	31.4	< 0.05

The backscattering spectra were obtained by means of a proportional counter through which a mixture of He–5% methane or of Ar–10% methane flowed to detect conversion electrons (CEMS) or backscattered X-ray (CXMS), respectively. It was thus possible to obtain information on surface layers up to 200 nm thick (CEMS) or up to 20 μm thick (CXMS) owing to the different escape depth of the two types of radiation. A standard least squares minimization routine was used to give the best-fit of a number of Lorentzian line-shapes.

3. Results

The X-ray analysis results, reported in Table II, which disagree with those of Holden and coworkers [7], will be clarified in the next section. The disagreement for non-deformed samples is probably due to differences in the mean composition.

Figs. 1 to 5 show some of the Mössbauer spectra obtained. Fig. 1 shows the difference between the A-type samples of the X1Mn16 alloy undeformed (Fig. 1a) and deformed by 64% (Fig. 1b): the work-hardening effect is deduced from the increase in the ferromagnetic (α' phase) components at the expense of the central paramagnetic peak (ϵ-phase). Fig. 1c shows the CEMS spectrum of the same unthinned alloy, deformed by 64% and characterized only by superimposed magnetic sextets. Clearly, there is a different phase distribution between bulk and surface corresponding to an apparently greater work-hardening of the surface layers. Spectra in Fig. 2 of X1Mn16 B-type samples with different deformations are representative of an intermediate state between surface and bulk.

Analogous effects of deformation on the X1Mn23 alloy are reported in Fig. 3. The

TABLE II X-Ray analysis results

Alloy	Deformation	Phases		
		γ	ϵ	α'
X1Mn16	0	+	++	++
	50		+	+++
X1Mn23	0	++	++	
	50		+++	++
X1Mn30	0	+++		
	50	+	++	++

+ traces.
++ relatively large presence.
+++ preponderance.

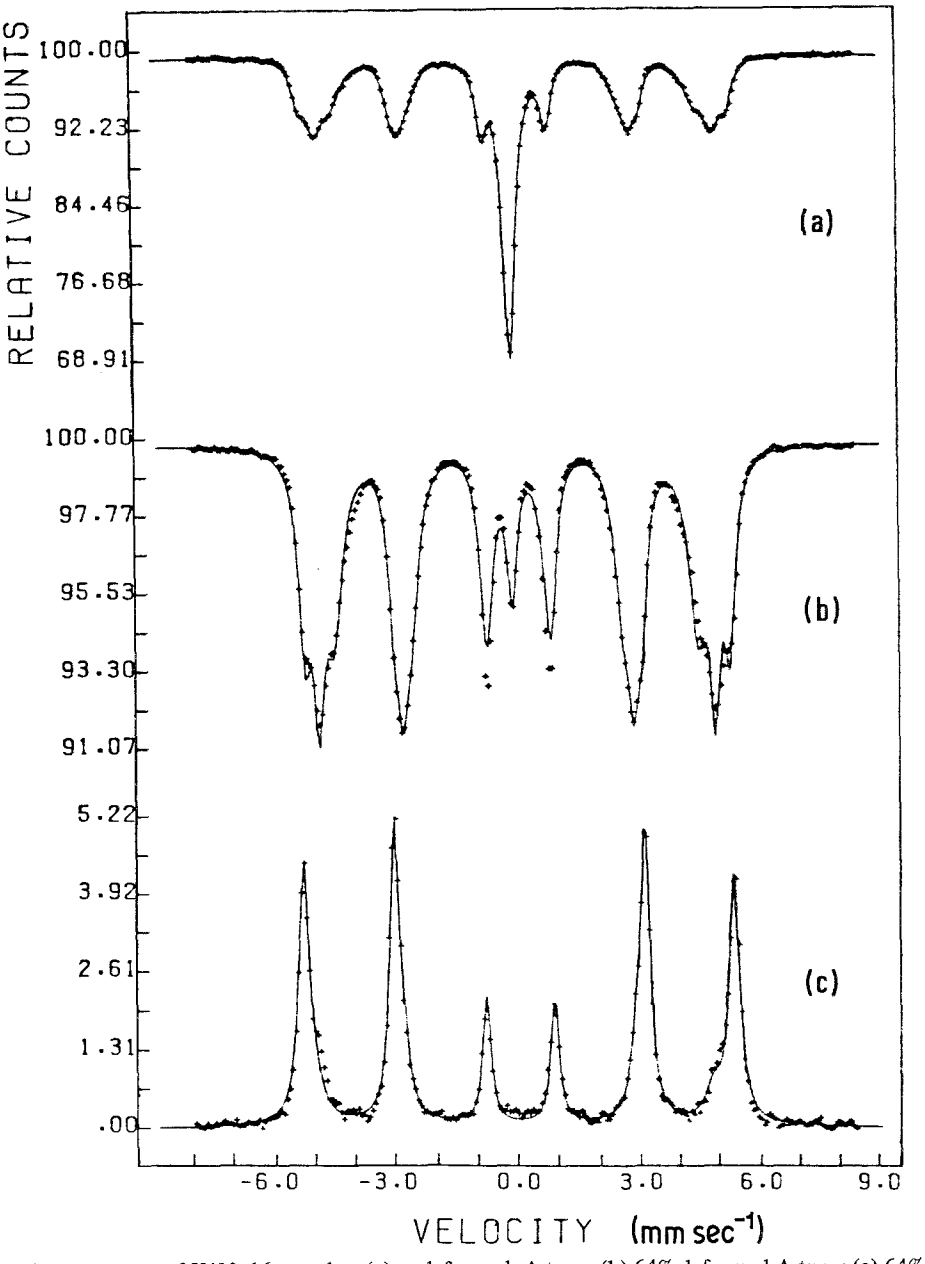

Figure 1 Mössbauer spectra of X1Mn16 samples: (a) undeformed, A-type; (b) 64% deformed A-type; (c) 64% deformed C-type (CEMS).

modifications in bulk structure are observable in Figs. 3a and b with the almost complete transformation $\gamma \rightarrow \epsilon$ at high deformation, whereas the spectra of Figs. 3c and d for B-type samples with different deformations show that even in this alloy the major effect of work-hardening is apparently localized at the surface. The CEMS and CXMS spectra reported in Figs. 4a and b, respectively, for the highly deformed alloy allow us to ascertain the presence of a different phase distribution in a surface layer of thickness about 200 nm with respect to a surface layer of thickness about 20 μm. In Fig. 4a, indeed, the paramagnetic component attributed to the ϵ-phase is practically absent, whereas it is relatively large in Fig. 4b.

The effect of bulk deformation is also verifiable for the X1Mn30 alloy from Figs. 5a and b, and so too, from Fig. 5c, is the apparent major work-hardening at the surface. The sequence of the

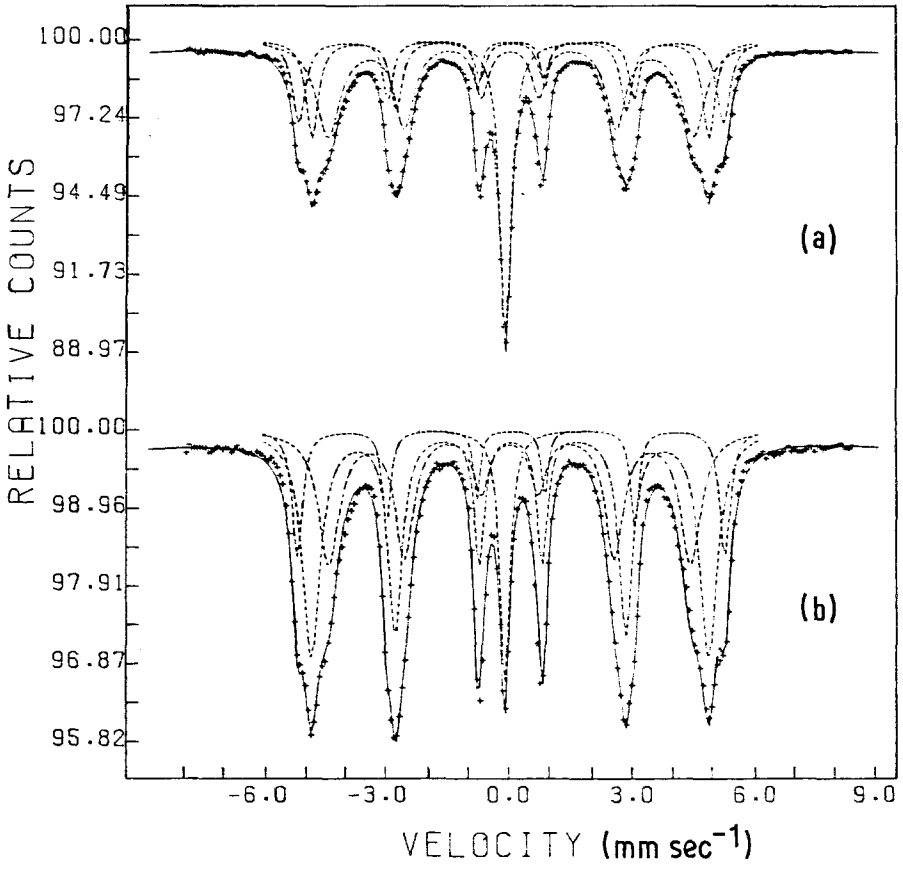

Figure 2 Mössbauer spectra of X1Mn16 samples: (a) 31% deformed B-type; (b) 64% deformed B-type.

spectra in Figs. 6a and b and Fig. 5b shows how the phase distribution changes from the surface to the bulk.

Table III gives the computed relative areas of the spectral components associated with the various phases present in the examined samples, according to the structural examinations of Table II. Details on the Mössbauer hyperfine parameters of the identified components are given as follows.

The antiferromagnetic fcc γ phase in X1Mn23 and X1Mn30 alloys is an unresolved sextet with isomer shift $\delta = -0.10 \pm 0.02\,\text{mm sec}^{-1}$ for both alloys, whereas the internal field H_{int} is slightly greater in the latter: 31.6 ± 0.5 kG instead of 29.6 ± 0.3 kG.

The hcp ϵ phase may be identified by a singlet with $\delta = -(0.12 \pm 0.17)\,\text{mm sec}^{-1}$ instead of a doublet with the same isomer shift and a very small quadrupole splitting as reported in [3].

The bcc α' phase is a superposition of at least three sextets, each one corresponding to a different Fe–Mn coordination [5]. The isomer shift is close to zero for each sextet and the measured average internal fields are, e.g. for the X1Mn16 alloy examined, 275.5, 302.2 and 325.3 kG.

As a first approximation the relative subspectra areas are proportional to the number of iron nuclei for a given configuration associated to the correspondent spectral component if: (a) the thickness of samples analysed in transmission geometry corresponds to a natural iron content not greater than 10 to $20\,\text{mg cm}^{-2}$ (thin absorber approximation); (b) the recoil-free fraction of ^{57}Fe is the same for the various phases. In the following, when referring to the phase percentage, we will deal with the normalized relative areas of the corresponding components.

4. Discussion

The evolution of the phase distribution in the bulk against deformation is shown in the diagrams of Fig. 7 obtained from Table III for the A-type samples. As foreseeable the work-hardening produces an abrupt increase of α' at expense of ϵ in the X1Mn16 alloy, a much greater increase of ϵ at expense of γ in the X1Mn23 alloy, whereas in the

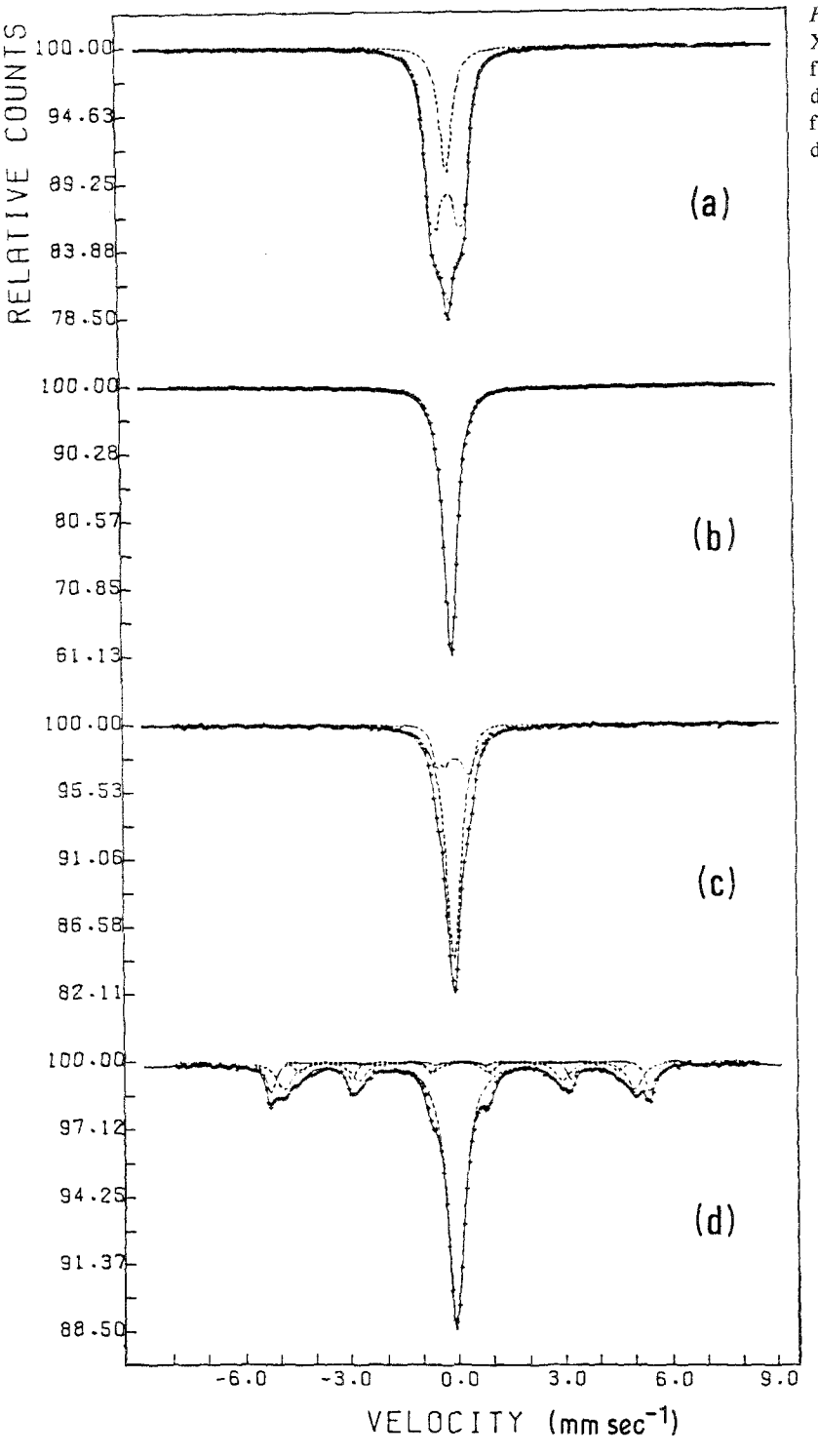

Figure 3 Mössbauer spectra of X1Mn23 samples: (a) undeformed A-type; (b) 50% deformed A-type; (c) 20% deformed B-type; (d) 50% deformed B-type.

X1Mn30 alloy, even at high deformation the maximum obtainable ϵ is about 7%. In both the X1Mn23 and X1Mn30 alloys the work-hardening does not produce α' in the bulk, but there are traces observed in the X-ray diffraction pattern of the highly deformed X1Mn30.

The situation considering the data at the surface is very different, as mentioned in the previous section. The C-type unthinned samples were analysed with the CEMS and the CXMS techniques which give the average situation in surface layers of thickness up to 200 nm and up to 20 μm,

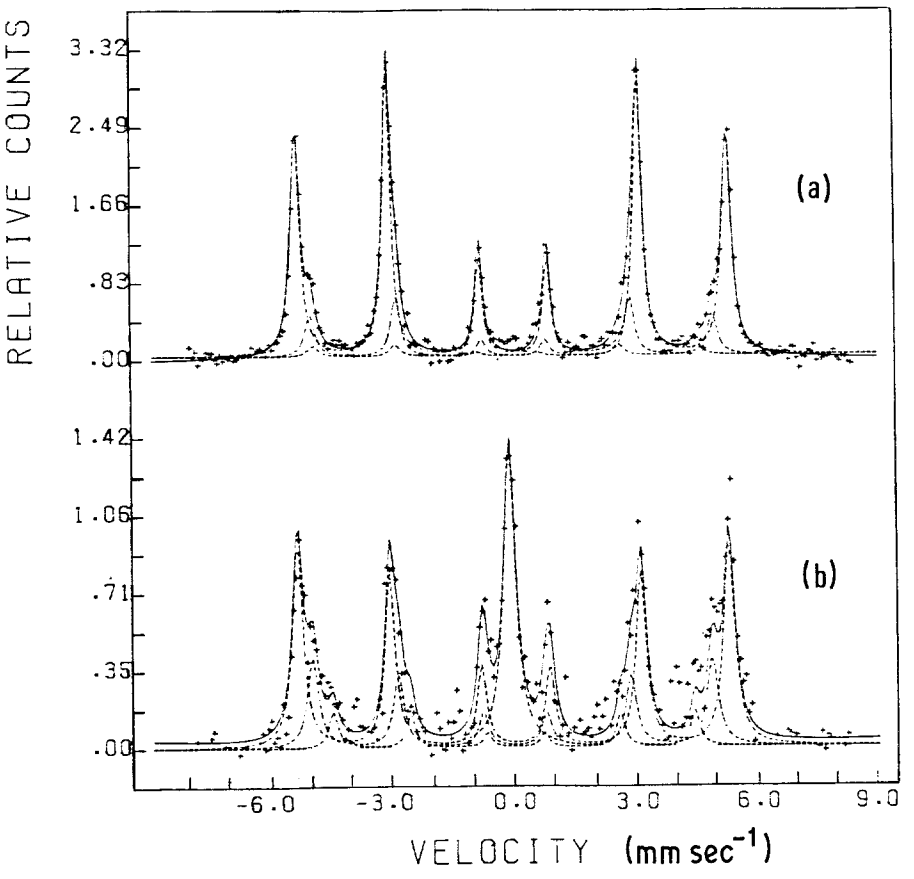

Figure 4 Mössbauer spectra of X1Mn23 samples: (a) 50% deformed C-type (CEMS); (b) 50% deformed C-type (CXMS).

respectively. By analysing B-type samples (thinned only on one side) average structural information on a layer of about 50 μm is also obtained. It is thus possible to construct the diagrams of Fig. 8 which clearly show the phase distribution from the surface to the bulk. The formation of a great amount of α', limited to a surface layer of about 50 μm in the X1Mn30 alloy (Fig. 8b), is quite unexpected whereas in the X1Mn23 alloy the formation of α' is observed only at high deformation and, at the same examined thickness to a smaller extent than in the X1Mn30 alloys (Figs. 7a and b). It is to be noted that the deformation-induced behaviour of the X1Mn23 alloy in the surface region differs from that of the X1Mn30 one: in the X1Mn23 α' is not detected at mean deformations, whereas the X1Mn30 has approximately the same behaviour at high and at mean deformations.

The reason for the observed trends may come from a different composition between surface and bulk, due to manganese evaporation during the intermediate annealings necessary to prepare the plates from which samples were obtained to be subsequently cold-worked. The compositions of Table I, determined by chemical analysis, are to be intended as average compositions of the full thickness for each plate obtained. In order to confirm the above assumption we examined the structure of the α' phase in some detail by considering the computed Mössbauer hyperfine parameters of the subspectra, taking into account their relative intensities I_1, I_2 and I_3 and the associated hyperfine magnetic fields H_1, H_2 and H_3. Barton *et al.* [5] found for their 12% Mn samples that the fields H_2 and H_3 decreased by 6.6% and by 13.8%, respectively, as compared with H_1. On the basis of [8] (according to which one manganese nearest neighbour cause a decrease in the magnetic hyperfine filed of the iron atom of 7.6%, the influence of the next-nearest manganese neighbour being only of 2.2%), they assumed that subspectrum 1 originates from iron atoms without nearest manganese neighbours, subspectrum 2 from iron atoms with one nearest manganese neighbour and subspectrum 3 from iron atoms with two or three nearest manganese neighbours. Our average results are

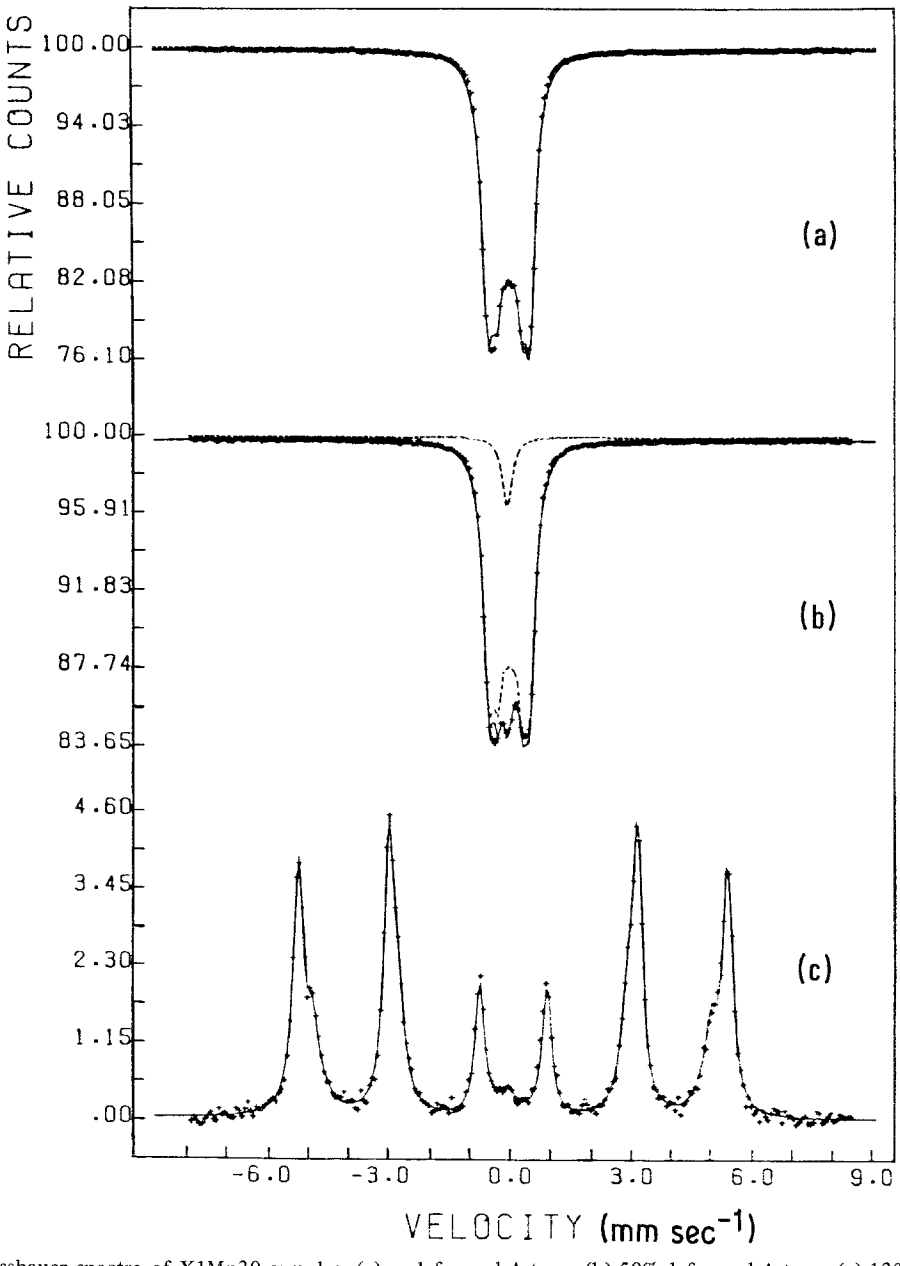

Figure 5 Mössbauer spectra of X1Mn30 samples: (a) undeformed A-type; (b) 50% deformed A-type; (c) 13% deformed C-type (CEMS).

$\Delta H_{2,1}/H_1 = 7.3\%$ and $\Delta H_{3,1}/H_1 = 15.5\%$, in good agreement with Stearns's [8] interpretation.

Let us now consider the hypothesis of a completely random distribution of the manganese atoms in the substitutional solid solution. By generalizing the considerations in [9], the probability p_i of having i nearest manganese neighbours among z nearest neighbour of an iron atom is

$$p_i = C_i^z x^i (1-x)^{z-i}$$

where

$$C_i^z = z!/[i!(z-i)!]$$

is the number of combinations of z objects taken i at a time, x is the manganese concentration, and z, the coordination number = 8 in the bcc structure.

By comparing p_i in Table IV and the measured I values in Table V, we find that our samples deviate from the statistical distribution, especially the X1Mn23 and X1Mn30 ones. Barton *et al.* [5] observed a similar behaviour and, in addition, a variation of the manganese distribution in annealed samples. This variation has been linked to the formation of ϵ and γ phases which should occur in

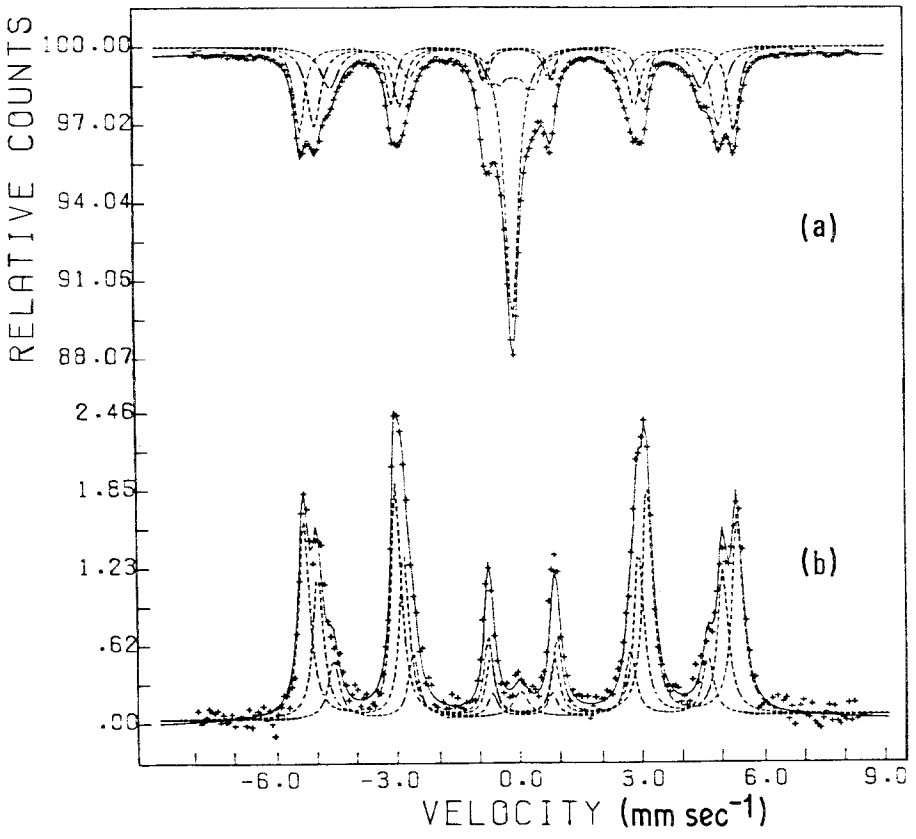

Figure 6 Mössbauer spectra of X1Mn30 samples: (a) 22% deformed B-type; (b) 22% deformed C-type (CEMS).

TABLE III Structural composition by Mössbauer spectroscopy of all studied samples. Upper limit of uncertainty on the reported values was estimated to be ± 2 per cent

Alloy	Deformation	Sample type	Geometry	Phases			Figure
				γ	ϵ	α'	
X1Mn16	0	A	transmission	4	28	68	1a
	22	A	transmission		20	80	
	64	A	transmission		5	95	1b
	31	B	transmission		16	84	2a
	64	B	transmission		7	93	2b
	31	C	CEMS		8	92	
	64	C	CEMS			100	1c
X1Mn23	0	A	transmission	76	24		3a
	22	A	transmission	10	90		
	50	A	transmission	3	97		3b
	20	B	transmission	32	68		3c
	50	B	transmission		58	42	3d
	20	C	CEMS		100		
	50	C	CEMS			100	4a
	50	C	CXMS		20	80	4b
X1Mn30	0	A	transmission	100			5a
	36	A	transmission	93	7		
	50	A	transmission	91	7	2	5b
	22	B	transmission	7	25	68	6a
	50	B	transmission	8	27	65	
	13	C	CEMS		3	97	5c
	22	C	CEMS		2	98	6b
	22	C	CXMS		10	90	
	50	C	CEMS		2	98	

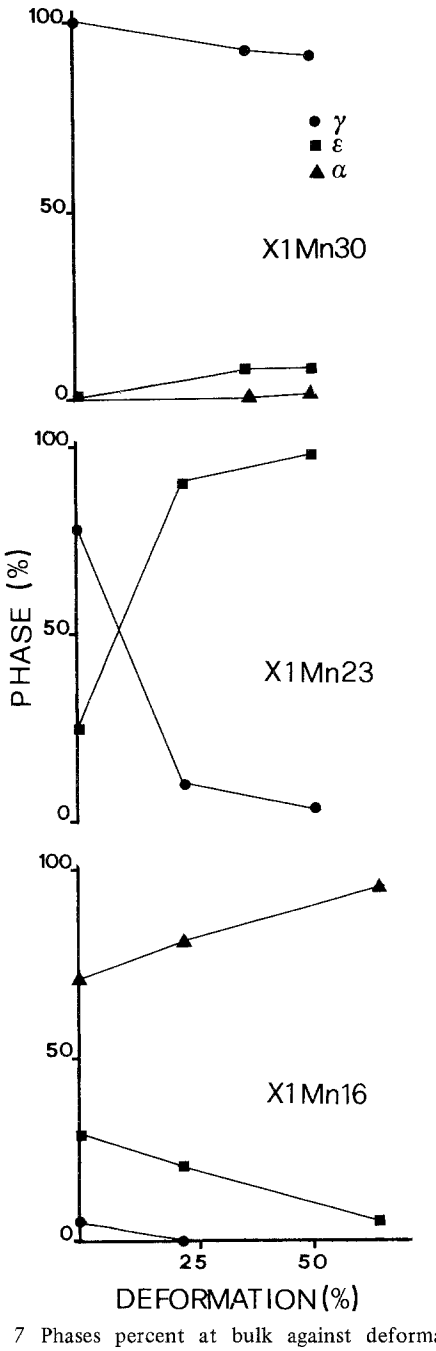

Figure 7 Phases percent at bulk against deformation degree as evaluated from Mössbauer spectra: (a) X1Mn16; (b) X1Mn23; (c) X1Mn30.

the manganese-rich regions with a greater probability of iron atoms with more than one nearest manganese neighbour. The behaviour of our X1Mn23 and X1Mn30 samples shows a tendency to an increase of I_1 with deformation; this is more marked in the spectra representative of the surface. This transformation, opposite to the one of

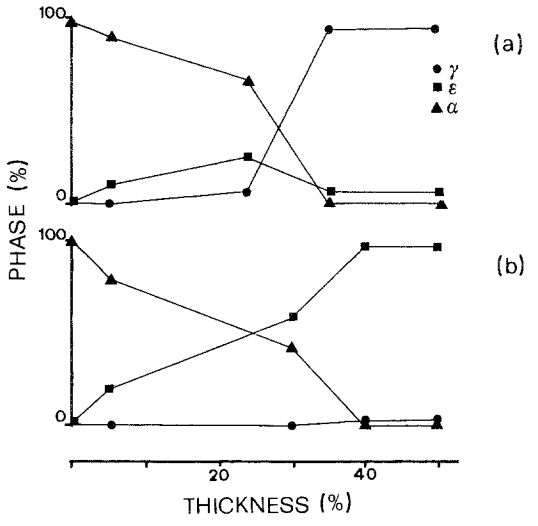

Figure 8 Phases distribution from the surface to the bulk as evaluated from Mössbauer spectra: (a) 50% deformed X1Mn23; (b) 22% deformed X1Mn30.

[5], should occur more easily from a γ phase near an ϵ one, which presumably is manganese-richer. We conclude that the decrease of manganese content near to the surface, due to the preparation of our alloys and confirmed by microanalysis tests (not reported here), influences the observed transformations more than a possible enhanced localized hardening.

The obtained data may also help to clarify the mechanism of the martensitic transformation $\gamma \rightarrow \epsilon, \alpha'$. We find, indeed, that in the X1Mn23 alloy, with a starting structure $\gamma + \epsilon$, the transformation $\gamma \rightarrow \alpha'$ occurs only at the surface (manganese poor) at high deformations, whereas at lower deformations the transformation is $\gamma \rightarrow \epsilon$. In the X1Mn30 alloy, that initially has only the γ phase, α' is obtained at the manganese-poor surface even at low deformations. The conclusion is that, when ϵ

TABLE IV Probabilities p_i ($i = 1$ to 8) of having i manganese atoms among the 8 nearest neighbours of an iron atom, on the basis of a completely random distribution.

p_i	Alloy		
	X1Mn16	X1Mn23	X1Mn30
p_0	0.25	0.12	0.05
p_1	0.38	0.29	0.18
p_2	0.25	0.31	0.29
p_3	0.10	0.19	0.26
p_4	0.02	0.07	0.15
p_5	4×10^{-3}	0.02	0.06
p_6	3×10^{-4}	3×10^{-3}	0.01
p_7	2×10^{-5}	2×10^{-4}	2×10^{-3}
p_8	5×10^{-7}	9×10^{-6}	9×10^{-5}

TABLE V Normalized relative intensities I_1, I_2 and I_3 of the α' subspectra for the alloys considered (C* refers to CXMS spectra)

Alloy	Sample type	Deformation	I_1	I_2	I_3
X1Mn16	A	0	22	38	40
	A	22	31	44	25
	A	64	27	32	41
	B	31	22	27	51
	B	64	18	43	39
	C	31	27	33	40
	C	64	18	47	35
X1Mn23	B	50	34	54	12
	C	50	78	18	4
	C*	50	68	23	11
X1Mn30	A	50	37	34	29
	B	22	41	47	17
	B	50	34	30	36
	C	13	66	19	15
	C	22	50	36	14
	C*	22	56	33	12
	C	50	46	38	17

exists prior to the deformation, the $\gamma \rightarrow \epsilon$ transformation is favoured at expenses of the $\gamma \rightarrow \alpha'$ one.

Acknowledgements

The support of the Italian Consiglio Nazionale delle Ricerche–Pragetto finalizzato "Metallurgia" through contract 82.01884.50 is gratefully acknowledged. The authors would also like to thank Professor E. Ramous for helpful discussions.

References

1. Y. ISHIKAWA and Y. ENDO, *J. Phys. Soc. Jpn.* **23** (1967) 205.
2. G. N. BELOZERSKIY, V. N. GITTSOVICH, V. N. KRAMAR, O. G. SOKOLOV and YU. P. KHIMICH, *Fiz. Metal. Metalloved.* **35** (1973) 472.
3. H. OHNO and M. MEKATA, *J. Phys. Soc. Jpn.* **31** (1971) 102.
4. V. S. LITVINOV, V. V. OVCHINNIKOV, S. P. DOVGOPOL and S. D. KARAKISHEV, *Fiz. Metal. Metalloved.* **47** (1979) 96.
5. J. BARTON, E. WIESER and M. MÜLLER, *Phys. Status Solidi (a)* **39** (1977) 259.
6. F. GAUZZI and B. VERDINI, *Metall. Ital.* **68** (1975) 623.
7. A. HOLDEN, J. D. BOLTON and E. R. PETTY, *JISI* **209** (1971) 721.
8. M. B. STEARNS *Phys. Rev.* **147** (1966) 439.
9. J. M. R. GENIN and P. A. FLINN, *Trans. AIME* **242** (1968) 1419.

Received 17 March
and accepted 24 March 1983